Permeability relation with other petrophysical parameters for periodic porous media

Keh-Jim Dunn*, Gerald A. LaTorraca*, and David J. Bergman‡

ABSTRACT

We modeled permeability (k) estimation based on porosity (ϕ), electrical formation factor ($\mathcal{F}$), and nuclear magnetic resonance (NMR) relaxation time (T), using periodic structures of touching and overlapping spheres. The formation factors for these systems were calculated using the theory of bounds of bulk effective conductivity for a two-component composite. The model allowed variations in grain consolidation (degree of overlap), scaling (grain size), and NMR surface relaxivity. The correlation of the permeability (k) with the predictor $aT^b\mathcal{F}^c$ was slightly higher than $aT^b\phi^c$ (i.e., a correlation coefficient of 0.98 versus 0.95). The exponent b ranged from 1.4 for a pure grain consolidation system to 2 for a pure scaling system. Variations in surface relaxivity are shown to cause significant scatter in the correlations.

INTRODUCTION

The permeability of a subsurface formation is a very important parameter in the petroleum industry for estimating producible hydrocarbon. Continuous direct measurements of permeability in boreholes is currently impractical. Consequently, well log measurements of other petrophysical parameters (porosity, formation factor, nuclear magnetic resonance (NMR) relaxation times, mineral compositions, Stoneley wave attenuation, etc.) are used to estimate permeability (Timur, 1969; Herron, 1987; Kenyon et al., 1988; Sen et al., 1990; Tang et al., 1998). These estimations are based largely on empirical correlations.

Permeability has been empirically correlated with porosity, formation factor, and surface-to-volume ratio, assuming that permeability is controlled by pore volume, pore throat size, and surface area (Walsh and Brace, 1984; Johnson et al., 1986; Katz and Thompson, 1986; Blair et al., 1996). Although various aspects have been studied to help understand the physics of the transport properties of rocks, the primary goal has been to estimate permeability from logs (Brown, 1972). NMR log measurements have been used extensively to predict permeability, assuming that the dominant NMR relaxation time of fluid-saturated rocks is related to the surface-to-volume ratio of the pore space. It is the purpose of the present paper to re-examine these correlations for permeability using periodic structures where all the necessary parameters can be calculated.

Two commonly used correlation schemes are $k = aT^b\mathcal{F}^c$ and $k = aT^b\phi^c$, where k is the permeability, T the NMR relaxation time, ϕ the porosity, and $\mathcal{F}$ the formation factor. The fitting constants (a, b, and c) are often empirically determined from core measurements. However, few attempts have been made to understand the physical meaning of these fitting constants, what properties of the rocks affect them, or if there is a fundamental relationship between these parameters. The periodic arrays of identical spheres offer a unique opportunity for such an investigation, because all the petrophysical quantities in the correlations (i.e., permeability, porosity, formation factor, NMR relaxation times, etc.) can be computed with high accuracy. Thus, these empirical formulas can be studied theoretically with controlled variation of the affecting factors. We varied the size scale, the surface relaxation strength, and the degree of consolidation, and computed their effects on the empirical formulas for the permeability.

We considered periodic porous systems of simple cubic (sc), body-centered cubic (bcc), and face-centered cubic (fcc) arrays of touching and overlapping spheres. The computation of porosity for these structures is based on a simple geometric consideration. The formation factor is calculated using a method proposed by Bergman and Dunn (1992). The NMR relaxation time for most clastics is given by $V_p/(\rho S)$, where V_p is the volume of the pore space, S is the surface area of the pore-matrix interface, and ρ is the surface relaxation strength. The values of permeability are taken from Larson and Higdon (1988).

Our paper is organized as follows. The next section reviews the calculation of a formation factor. The third section discusses various schemes of correlating these theoretically computed

petrophysical parameters. Section four uses real rock data for the analysis. Section five summarizes our present findings.

COMPUTATION OF FORMATION FACTOR

We used the method of Bergman and Dunn (1992) to compute the formation factor for periodic porous media. We calculated moments of the pole spectrum of a two-component composite to produce a continued fraction expansion for the bulk effective dielectric constant or electrical conductivity. Then, we used the rigorous bounds for the bulk effective conductivity to determine the formation factor for the composite. A more detailed discussion of the computation method is given in the Appendix.

The upper and lower bounds of the bulk effective conductivity for the composite usually converge very quickly, as the number of moments used in the calculation increases, to nearly the same value when the conductivity contrast between the two components of the composite is small. When the conductivity contrast becomes large, such as the case for computing the formation factor, the two bounds diverge from each other. However, the lower bound converges to the true bulk effective conductivity for the composite. This is corroborated by computing the bulk effective conductivity of the same composite by switching the values of conductivity of the matrix and pore space, as discussed in the Appendix. Recent work of Helsing (1996) and Cheng and Greengard (1997) have also dealt with similar problems of computing electrostatic fields of two-component composites, but with different approaches.

The formation factors we computed for three different periodic structures (simple cubic, body-centered cubic, and face-centered cubic arrays for identical touching and overlapping spheres) are shown in Figure 1. We found results of our calculation are quite consistent with those of Schwartz and Kimminau (1987), who used the network simulation and minimum area approximation approaches. The formation factors calculated by Shen et al. (1990) tend to be smaller at low porosity values. This is because they used a Fourier expansion

FIG. 1. Formation factor as functions of porosity for sc, bcc, and fcc periodic structures of identical touching and overlapping spheres.

method with only $N = 1$ in the reciprocal space (N is a measure of the size of the reciprocal space over which the Fourier expansion is carried out; see the Appendix). The convergence of the Fourier expansion method has been shown to be reasonably fast for porosities where spheres just touch or slightly overlap with each other, but becomes quite slow for lower porosities where many higher order Fourier expansion terms are needed (Bergman and Dunn, 1995a). Our present calculation used a Fourier expansion with N up to 21 in the reciprocal space.

PERMEABILITY FOR PERIODIC POROUS MEDIA

Theoretical computation of the permeability of periodic porous media has been studied extensively in the past using spherical harmonics (Hasimoto, 1959; Zick and Homsy, 1982; Sangani and Acrivos, 1982; Larson and Higdon, 1988). Here, we use Larson and Higdon's (1988) results for our analysis. Table 1 shows the results from Larson and Higdon, along with our calculation of formation factor and NMR relaxation times. The friction coefficient K, given by Larson and Higdon,

$$K = \frac{f}{6\pi\mu RU} \tag{1}$$

is a dimensionless quantity, where f is the force on a single inclusion, μ is the fluid viscosity, R is the radius of the sphere, and U is the superficial or average velocity through the lattice. The permeability k is defined by

$$k \equiv \frac{\mu U V_0}{f} = \frac{V_0}{6\pi RK}, \tag{2}$$

where V_0 is the total volume per inclusion. The permeability defined in this way has dimensions of $(length)^2$. In Table 1, we show values of the dimensionless permeability k/d^2, where d is the edge length of the cubic unit cell of the Bravais lattice. The values quoted from Larson and Higdon include only those for touching and overlapping spheres and exclude those with very small porosities where the corresponding permeabilities are less than 0.1 md for $d = 10 \mu$m.

We calculated NMR relaxation times assuming that surface relaxation is the dominant mechanism for polarization decay and that bulk relaxation can be ignored. The dominant NMR relaxation rate in the porous medium has been shown (Brownstein, and Tarr, 1979; Mitra and Sen, 1992; Bergman and Dunn, 1995a) to be equal to $\rho S/V_p$ when $\rho d/D$ is small (i.e., the fast diffusion regime), and D is the diffusion constant for water. Hence, the dominant NMR relaxation time is calculated as $V_p/\rho S$ and shown in Table 1 as T_1. We computed these T_1 values (in milliseconds) assuming a surface relaxation strength $\rho = 10^{-3}$ cm/s and evaluating V_p and S directly for the case of $d = 10 \mu$m. Here, we do not make the distinction between the longitudinal relaxation time T_1 (for which ρ_1 should be used) and the transverse relaxation time T_2 (for which ρ_2 should be used) (Kleinberg et al., 1994). In general, as the Larmor frequency gets lower, T_2 is quite close to T_1, except that T_2 may be diffusionally shortened by induced internal field gradients or an externally applied field gradient. The strength of the induced internal gradients depends on the magnetic susceptibility contrast between solid and pore fluid (Bergman and Dunn, 1995b).

Figure 2 shows the permeability as a function of porosity for sc, bcc, and fcc sphere arrays, where we have also included large
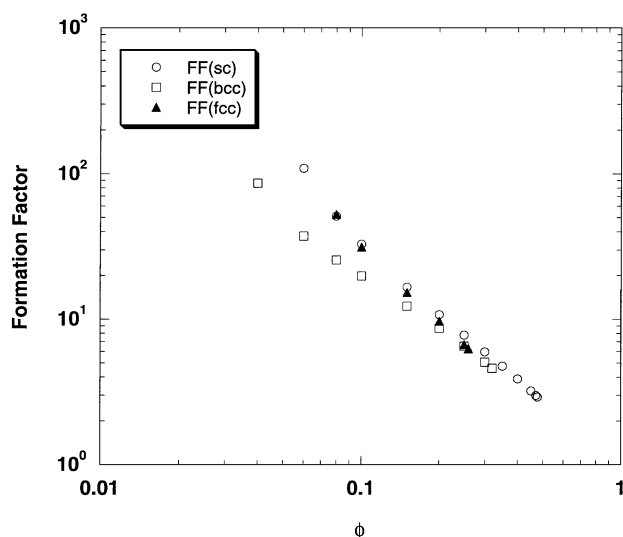
porosity values for which the spheres do not touch. Evidently, porosity alone is not a very good parameter for characterizing the permeability because the points arising from the different structures do not lie on a single curve, even in regions of high porosity, where they exhibit the same power law dependence on ϕ.

Figure 3 shows the result of using the form $aT^b\phi^c$ to represent permeability. Here, we have included only porosities for which the spheres are touching or overlapping. The permeability is computed using an edge length for the Bravais lattice of 10 μm. The fitting constants are $a = 1.024$, $b = 1.404$, and $c = 2.139$, with a correlation coefficient $r^2 = 0.942$. Note that the data sets we used are different packings of identical spheres where we achieved the porosity reduction by increasing the amount of overlap between neighboring spheres. This grain consolidation process reduces permeability and provides the dynamic range for the permeability shown in Figure 3. However, such a dynamic range for permeability can also be achieved at a fixed porosity by simply varying the overall size scale. In the latter case, the permeability would simply vary as the square of the length scale.

Figure 4 shows the results of such a change of size scale where the data sets include those of Figure 3 and the scaled data sets for edge lengths 30, 60, and 100 μm. Using the same functional form, $aT^b\phi^c$, the fitting constants now become $a = 0.120$, $b = 1.853$, and $c = 1.833$, with a correlation coefficient $r^2 = 0.952$. Notice that the constant b changes from 1.404 to 1.853, from pure grain consolidation to both grain consoli-

dation and scale change. In the functional form $aT^b\phi^c$, T is the only parameter that depends on the length scale (T is simply proportional to that scale). If the permeability changes were entirely due to the scale change, the exponent for T would be exactly 2. Naturally, the b value for the pure consolidation case depends on our model for the periodic structures. The b value for the real rock systems may be different. However, this exercise elucidates how the grain consolidation and the size scaling affect the value of the exponent b.

Kenyon et al. (1988) and Banavar and Schwartz (1987) used $a = 1.0$, $b = 2.0$, and $c = 4.0$. Figure 5 shows that for these constants, the correlation coefficient r^2 becomes 0.913, and the correlation is not as good as that shown in Figure 4, especially at the higher permeabilities. Comparing Figure 5 with Figure 4, the change in the exponent c seems quite significant. In fact, such a large change is tolerated because the correlation coefficient is only decreased very slightly: the reduction in the factor ϕ^c by increasing c is mostly offset by the modest increase of the exponent b in T^b. This shows that T and ϕ are not independent parameters in characterizing the permeability.

So far, we have assumed a constant surface relaxivity $\rho = 10$ μm/s in our calculation. For real rocks, values of ρ range from 10 to 1 μm/s (Kenyon et al., 1988; Kleinberg et al., 1994). Figure 6 shows the results of varying ρ where we use the result of Figure 3 for a unit cell edge length of 10 μm but with surface relaxation strength ranging from 10 to 1 μm/sec. Since there is no scale change, the permeability value remains the same as the surface relaxivity changes. This broadens the range of

Table 1. Theoretically computed permeability from Larson and Higdon (1988) with the T_1 and the formation factor $\mathcal{F}$ for simple cubic, body-centered, and face-centered arrays of identical touching and overlapping spheres for different porosities from this work.

ϕ	Concentration	Friction Coefficient	Permeability* k/d^2	T_1	$\mathcal{F}$
Simple Cubic					
0.4726	0.5236	41.99	2.5269×10^{-3}	151.64	2.907
0.47	0.53	43.60	2.4237×10^{-3}	150.22	2.98
0.45	0.55	48.80	2.1380×10^{-3}	145.80	3.21
0.40	0.60	66.10	1.5288×10^{-3}	134.73	3.88
0.35	0.65	93.36	1.0480×10^{-3}	123.61	4.75
0.30	0.70	139.8	6.7718×10^{-4}	112.34	5.96
0.25	0.75	228.3	4.0080×10^{-4}	100.79	7.76
0.20	0.80	426.9	2.0681×10^{-4}	88.82	10.73
0.15	0.85	1.020×10^3	8.3276×10^{-4}	76.18	16.65
0.10	0.90	4.29×10^3	1.8951×10^{-5}	62.57	32.73
0.08	0.92	1.20×10^4	6.6396×10^{-6}	56.81	51.09
0.06	0.94	5.726×10^4	1.3599×10^{-6}	51.02	109
Body-Centered Cubic					
0.31982	0.68018	162.3	3.7675×10^{-4}	67.87	4.60
0.30	0.70	191.0	3.1761×10^{-4}	64.96	5.07
0.25	0.75	299.2	1.9772×10^{-4}	57.34	6.52
0.20	0.80	520.5	1.1072×10^{-4}	49.22	8.67
0.15	0.85	1.073×10^3	5.2253×10^{-5}	40.34	12.29
0.10	0.90	3.05×10^3	1.7846×10^{-5}	30.23	19.80
0.08	0.92	5.47×10^3	9.8253×10^{-6}	25.66	25.62
0.06	0.94	1.14×10^4	4.6519×10^{-6}	20.67	37.22
0.04	0.96	3.2×10^4	1.6325×10^{-6}	16.91	86.42
Face-Centered Cubic					
0.25952	0.74048	431.0	8.7038×10^{-5}	41.30	6.25
0.25	0.75	480.0	7.7816×10^{-5}	40.49	6.67
0.20	0.80	426.9	3.9916×10^{-5}	36.08	9.67
0.15	0.85	913.8	1.6077×10^{-5}	31.37	15.28
0.10	0.90	2.21×10^3	3.6879×10^{-6}	26.27	31.33
0.08	0.92	9.34×10^3	1.3694×10^{-6}	24.17	52.49

*The permeability is in dimensionless units. In order to get its value in md (millidarcys), the dimensionless value should be multiplied by d^2, where d is the unit cell size in μm (1 md $= 0.987 \times 10^{-3} \mu$m^2).

scatter even in the high permeability case, where our model showed very good data collapse when ρ is constant and small. Hence, we propose that in clastic sediments the breadth of scatter of the permeability data in the high-permeability regime is caused mainly by the wide range of values for the surface relaxivity.

Figure 7 shows the results when we take the data set of Figure 3 (i.e., the pure grain consolidation system) and plot permeability versus $aT^b\mathcal{F}^c$ instead of versus $aT^b\phi^c$. Figure 8 shows the results when we also include the size scaling effect, with the edge lengths of 10, 30, 60, and 100 μm. The calculated

exponents b and c in Figures 7 and 8 are quite consistent with those calculated in Figures 3 and 4 (where $aT^b\phi^c$ is used) if we apply the relation $\mathcal{F} \approx \phi^{-1.5}$ (as observed in Figure 1 for large porosities). However, the use of formation factor $\mathcal{F}$ instead of porosity ϕ significantly increases the correlation with permeability data. This is quite evident when comparing Figures 4 and 8 in the low permeability region, where data scatter is much less when $aT^b\mathcal{F}^c$ is used.

The concept of using the formation factor to correlate permeability is not new. Walsh and Brace's (1984) simple model of considering flow in a rock as a flow through a bundle of tubes
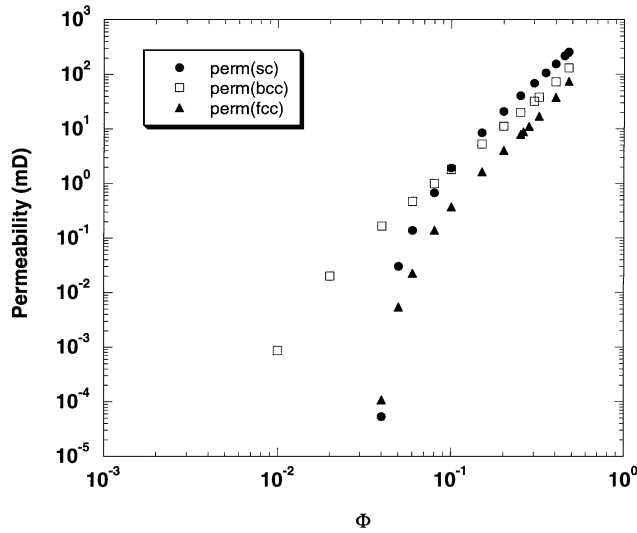

FIG. 2. Permeability as functions of porosity for periodic structures of sc, bcc, and fcc where we have included very high porosities where the spheres are not touching. The edge length of the Bravais lattice is 10 μm. Permeability is in millidarcys, where 1 md $= 0.987 \times 10^{-11}$ cm^2.

FIG. 4. Permeability versus $aT^b\phi^c$ for periodic structures of sc, bcc, and fcc using the data from Figure 3 (i.e., 10 μm) and the scaled data sets for 30, 60, and 100 μm. The length scale refers to the edge length of the Bravais lattice used in the computation. The fitting constants are $a = 0.120$, $b = 1.853$, and $c = 1.833$, with a correlation coefficient $r^2 = 0.95$.
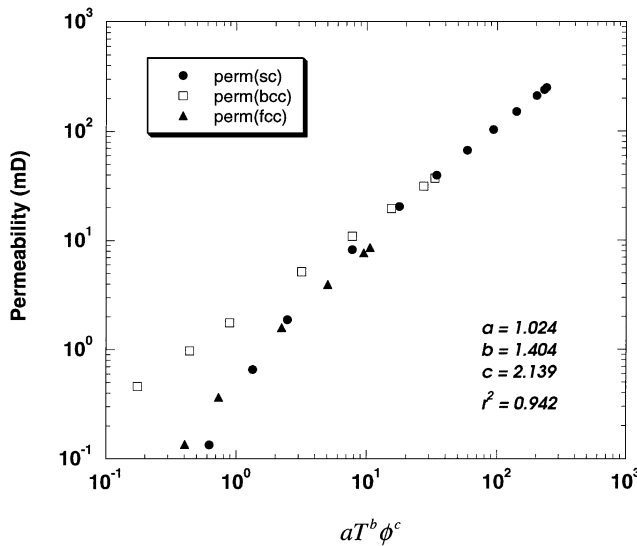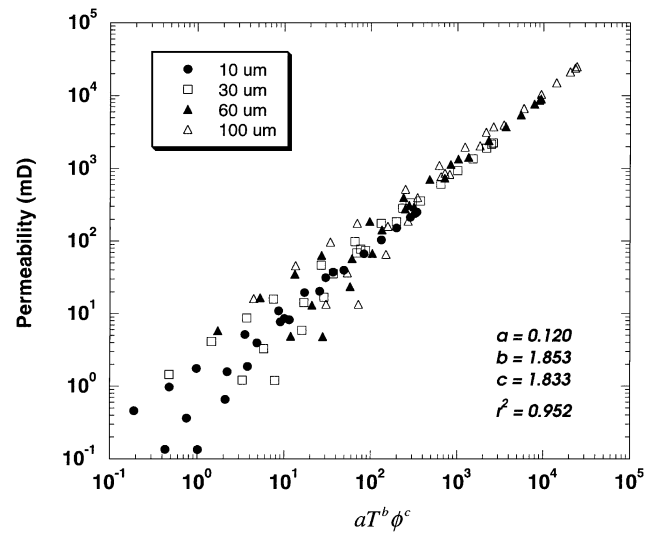

FIG. 3. Permeability versus $aT^b\phi^c$ for periodic structures of sc, bcc, and fcc using only porosities where the spheres are touching or overlapping. The edge length of the Bravais lattice is 10 μm. The fitting constants are $a = 1.024$, $b = 1.404$, and $c = 2.139$, with a correlation coefficient $r^2 = 0.94$.
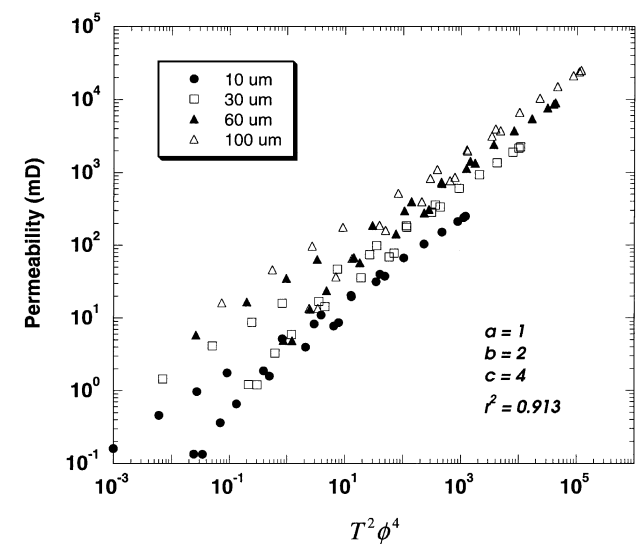

FIG. 5. Permeability versus $aT^b\phi^c$ for periodic structures of sc, bcc, and fcc using the data from Figure 4 but with fixed constants $a = 1.0$, $b = 2.0$, and $c = 4.0$. The correlation coefficient now becomes $r^2 = 0.91$.

yielded the permeability

$$k = (1/b)\phi^3 (V/A_s)^2 (1/\mathcal{F}), \qquad (3)$$

where b is a shape factor, A_s/V is the surface area per unit volume, and $\mathcal{F}$ is the formation factor. Katz and Thompson (1986), on the basis of a percolation argument, and Johnson et al. (1986), on the basis of the analogy between electrical and hydraulic conductions in porous media, proposed the following relationship:

$$k \sim L^2/\mathcal{F} = L^2\phi^m, \qquad (4)$$

where L is either the critical pore diameter in the mercury porosimetry measurements or the characteristic length in the electrical conduction for the porous medium. Blair et al. (1996) summarize the discussion on this subject in great detail.

We found that using the formation factor in computing the above described correlations does more than merely replacing ϕ^m by $1/\mathcal{F}$. From Figure 3, different values of m must be used for different structures when ϕ decreases below 0.1. This divergence of values of $\mathcal{F}$ corresponds to a similar divergence of values of the permeability at low permeabilities. Using $\mathcal{F}$ as the characteristic parameter improves collapse of the data in the low porosity–low permeability regime, as shown in Figures 4 and 8. Although our model demonstrated that in principle $aT^b\mathcal{F}^c$ is a better choice than $aT^b\phi^c$, in reality, other hetergeneous factors obscure the slight superiority in its correlation with the permeability, as discussed in the following section.

DISCUSSION OF REAL ROCK DATA

The real rock data present many heterogeneities and uncontrollable factors. The model systems we considered used identical spheres. To appy the results to real rock data, we need to determine significant and insignificant differences between real rocks and our models for the permeability correlations. We can think of the following:

1) Real rock systems are not identical spheres. They come in many different shapes and sizes. The packing is random, disordered, and certainly not periodic. This will significantly affect the formation factor, and hence the Archie's exponent m. However, we expect that the general relation such as $k \sim L^2/\mathcal{F} = L^2\phi^m$ holds for both the real rock systems and the periodic arrays of spheres, only the formation factor will be different. Thus, we expect our conclusion on the scaling effect on the fitting constant, exponent b, should hold for real rocks excluding other influencing factors.

2) The real rock systems certainly have different values of surface relaxation strength ρ. Within the zone probed by the NMR logging tool, variations in ρ can often be expected to be minimal. However, at larger scales, ρ can not be assumed to be constant. Large surface relaxivity caused by transition metal ions has been known to
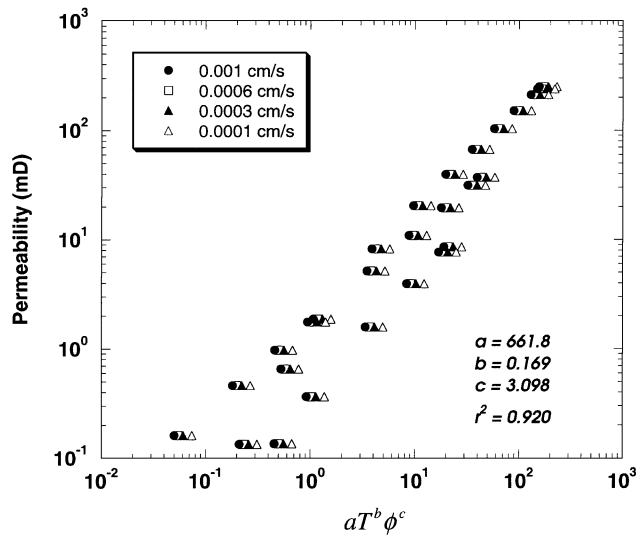

FIG. 6. Permeability versus $aT^b\phi^c$ for periodic structures of sc, bcc, and fcc with the surface relaxation strength ρ ranging from 0.001 to 0.0001 cm/s.
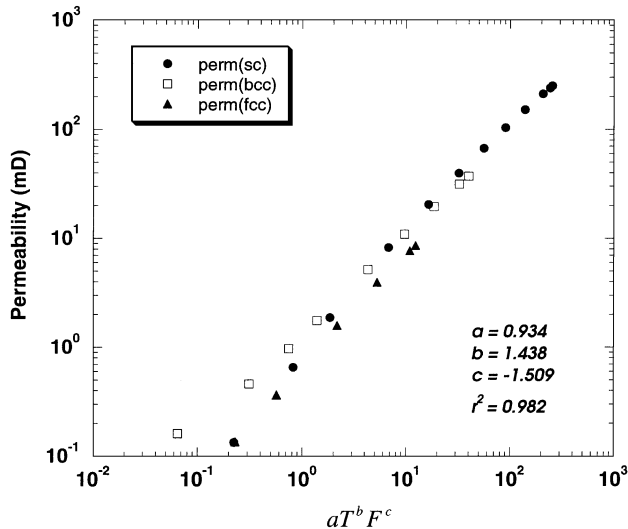

FIG. 7. Permeability versus $aT^b\mathcal{F}^c$ for periodic structures of sc, bcc, and fcc using the data from Figure 3.
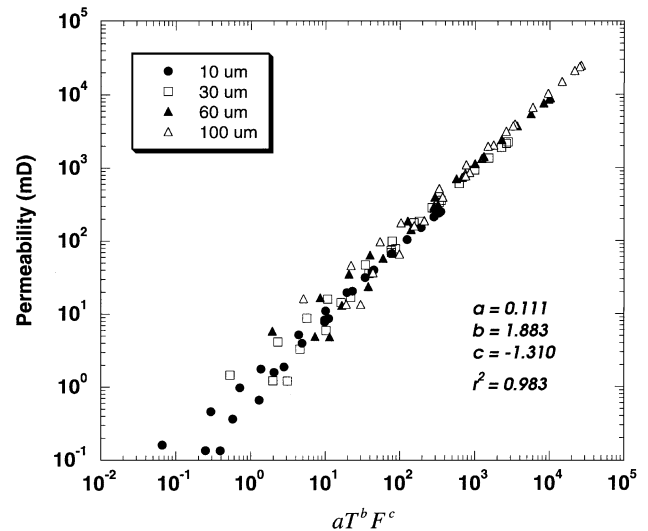

FIG. 8. Permeability versus $aT^b\mathcal{F}^c$ for periodic structures of sc, bcc, and fcc where using the data from Figure 4.

cause fast NMR relaxation and have very short relaxation times. Our conclusion on the variation of surface relaxivity causing the scattering in permeability crossplots is independent of our specific model. Hence, we believe that in real rock systems the scattering of data in the crossplots of core permeability with the permeability estimators is in large part due to the variability of ρ.

3) In our model, we have assumed a single dominant relaxation time given by $V_p/\rho S$. In real rock systems, we expect more than one dominant relaxation time. Usually, a geometric average of these relaxation times is used for the permeability correlation. However, depending on the diffusion coupling between large and small pores, two different length scales can show up either as two dominant relaxation times or as merged into one relaxation time (Ramakrishnan et al., 1998). This effect is in fact controlled by the factor $\rho d/D$ and, therefore, related to the variability of ρ. When the ρ becomes too small and the relaxation time $T = V_p/\rho S$ becomes large enough that the bulk relaxation of water is not negligible, the NMR relaxation time is no longer inversely proportional to the surface-to-volume ratio. All these uncertainties disrupt the correlation of permeability with the predictors $aT^b\phi^c$ and $aT^b\mathcal{F}^c$.

Figures 9 and 10 show the results for the two correlation schemes ($aT^b\phi^c$ and $aT^b\mathcal{F}^c$) for permeability of sandstones of 260 core samples from different parts of the world. The NMR relaxation times are T_{1G}, the geometric averages of T_1 over the distribution of relaxation times of each sample between 1 ms and 10 s measured at 10 MHz (LaTorraca et al., 1993). The fact that the exponent b is close to 2 shows that the data are mainly from rocks of different grain sizes. The large dynamic range of permeability is caused by size scaling rather than grain consolidation. This is indeed the case as shown in Figure 11 where, out of 260 data points, only 10 samples have porosity values below 0.1. Most of the samples have porosity values between 0.20 and 0.25.
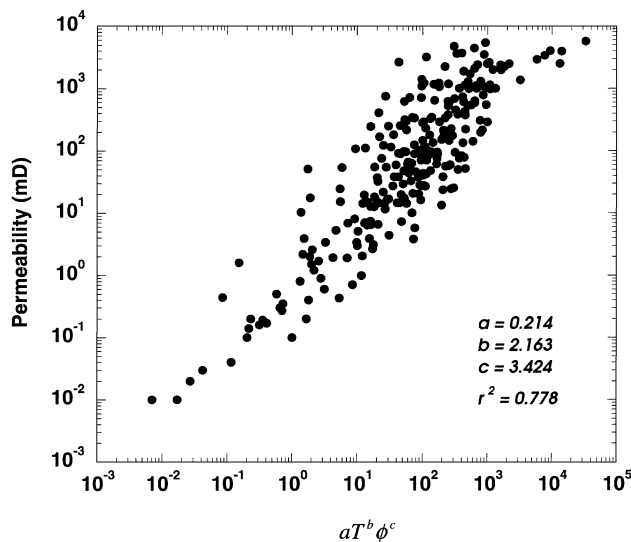
The large scatter of data points in these figures is, in our opinion, due to a large variation in surface relaxation strength among different samples.

As indicated by the correlation coefficients r^2 in Figures 9 and 10, the correlation scheme of $aT^b\mathcal{F}^c$ is slightly better than $aT^b\phi^c$, similar to our finding from model calculations in Figures 4 and 8.

SUMMARY

We have studied the correlation between theoretically computed permeability, porosity, formation factor, and NMR relaxation times for periodic porous media of identical touching and overlapping spheres. Although the systems that we consider are extremely idealized, this approach has the advantage of isolating each physical parameter, such as grain consolidation

FIG. 10. Permeability versus $aT^b\mathcal{F}^c$ for sandstones of real rock systems using the same set of data as in Figure 9.

a = 1.501
b = 2.053
c = -2.395
r² = 0.795

FIG. 9. Permeability versus $aT^b\phi^c$ for sandstones of real rock systems.
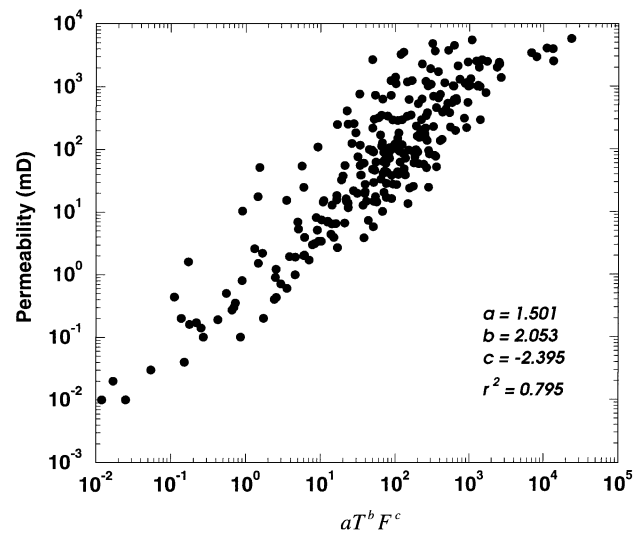
a = 0.214
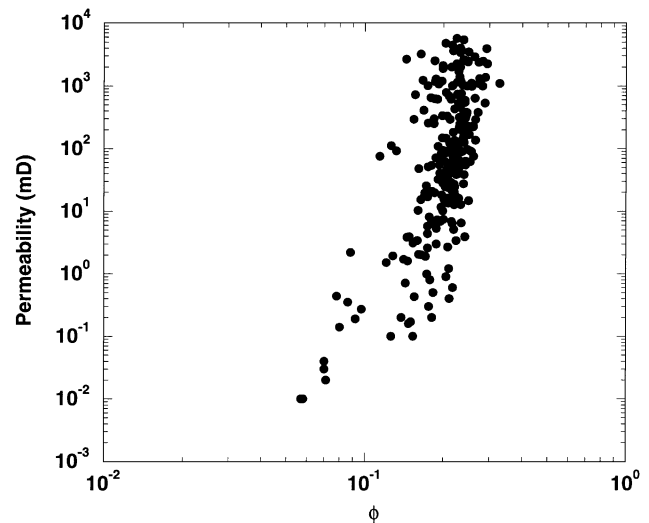*b = 2.163*
c = 3.424
r² = 0.778

FIG. 11. Permeability versus ϕ for sandstones of real rock systems using the same set of data as in Figure 9.

(porosity reduction), size scaling (size of the grain), and surface relaxation strength, and allowing us to study its implication and effects individually in the various correlation schemes. We have arrived at the following conclusions:

1) The form $aT^b\mathcal{F}^c$ generally provides slightly better correlation to permeability than $aT^b\phi^c$.
2) The exponent b for the relaxation time T ranges from 1.4 for pure grain consolidation systems to 2 for pure scaling change systems. Reservoir rocks often have a value near 2, indicating that the changes are due mainly to grain size change.
3) The scattering of data in the correlation of the permeability with the predictors $aT^b\phi^c$ and $aT^b\mathcal{F}^c$ appears to be due mainly to the variation in surface relaxation strength.
4) The form $aT^b\phi^c$ is relatively tolerant, especially for somewhat large variation of c. This happens because a large increase in c can be easily offset by a modest increase in b.

REFERENCES

Banavar, J. R., and Schwartz, L. M., 1987, Magnetic resonance as a probe of permeability in porous media: Phys. Rev. Lett., **58**, 1411–1414.
Bergman, D. J., and Dunn, K. J., 1992, Bulk effective dielectric constant of a composite with a periodic microgeometry: Phys. Rev., **B 45**, 13262–13271.
——— 1995a, Self-diffusion in a periodic porous medium with interface absorption: Phys. Rev., **E 51**, 3401–3416.
——— 1995b, NMR of diffusing atoms in a periodic porous medium in the presence of a nonuniform magnetic field: Phys. Rev., **E 52**, 6516–6535.
Blair, S. C., Berge, P. A., and Berryman, J. M., 1996, Using two-point correlation functions to characterize microgeometry and estimate permeabilities of sandstones and porous glass: J. Geophys. Res., **101**, 20359–20375.
Brown, R. J. S., 1972, Nuclear magnetism well logging method and apparatus: U. S. Patent 3 775 671.
Brownstein, K. R., and Tarr, C. E., 1979, Importance of classical diffusion in NMR studies of water in biological cells: Phys. Rev., **A 19**, 2446–2453.
Cheng, H., and Greengard, L., 1997, On the numerical evaluation of electrostatic fields in dense random dispersions of cylinders: J. Comput. Phys. **136**, 629–639.
Hasimoto, H., 1959, On the periodic fundamental solutions of the Stokes equations and their application to viscous flow past a cubic array of spheres: J. Fluid Mech., **5**, 317–328.
Helsing, J., 1996, Thin bridges in isotropic electroctatics: J. Comput. Phys. **127**, 142–151.
Herron, M., 1987, Estimating the intrinsic permeability of clastic sediments from geochemical data: 28th Ann. Logging Symp., Soc. Prof. Well Log Analysts, paper HH.
Johnson, D. L., Koplik, J., and Schwartz, L. M., 1986, New pore-size parameter characterizing transport in porous media: Phys. Rev. Lett., **57**, 2564–2567.
Katz, A. J., and Thompson, A. H., 1986, Quantitative prediction of permeability in porous rock: Phys. Rev., **B 34**, 8179–8181.
Kenyon, W. E., Day, P. I, Straley, C., and Willemson, J. F., 1988, A three-part study of NMR longitudinal relaxation properties of water-saturated sandstones: SPE Formation Evaluation, **3**, 622–636.
Kleinberg, R. L., Kenyon, W. E., and Mitra, P. P., 1994, Mechanism of NMR relaxation of fluids in rock: J. Mag. Reson., **A 108**, 206–214.
Korringa, J., 1984, The influence of pore geometry on the dielectric dispersion of clean sandstones: Geophysics, **49**, 1760–1762.
Korringa, J., and LaTorraca, G. A., 1986, Application of the Bergman-Milton theory of bounds to the permittivity of rocks: J. Appl. Phys., **60**, 2966–2976.
Larson, R. E., and Higdon, J. J. L., 1988, Periodic grain consolidation model of porous media: Phys. Fluids, **A 1**, 38–46.
LaTorraca, G. A., Dunn, K. J., and Brown, R. J. S., 1993, Predicting permeability from nuclear magnetic resonance and electrical properties measurements: 1993 Soc. Core Analysts Conf., paper 9312.
Mitra, P. P., and Sen, P. N., 1992, Effects of microgeometry and surface relaxation on NMR pulsed-field-gradient experiments: simple pore geometry: Phys. Rev., **B 45**, 143–156.
Ramakrishnan, T. S., Schwartz, L. W., Fordham, E. J., Kenyon, W. E., and Wilkinson, D. J., 1998, Forward models for nuclear magnetic resonance in carbonate rocks: 39th Ann. Logging Symp., Soc. Prof. Well Log Analysts, paper SS.
Sangani, A. S., and Acrivos, A., 1982, Slow flow through a periodic array of spheres: Internat. J. Multiphase Flow, **8**, 343–360.
Schwartz, L. W., and Kimminau, S., 1987, Analysis of electrical conduction in the grain consolidation model: Geophysics, **52**, 1402–1411.
Sen, P. N., Straley, C., Kenyon, W. E., and Whittingham, M. S., 1990, Surface-to-volume ratio, charge density, nuclear magnetic relaxation, and permeability in clay-bearing sandstones: Geophysics, **55**, 61–69.
Shen, L. C., Liu, C., Korringa, J., and Dunn, K. J., 1990, Computation of conductivity and dielectric constant of periodic porous media: J. Appl. Phys., **67**, 7071–7081.
Tang, X. M., Atunbay, M., and Shorey, D., 1998, Joint interpretation of formation permeability from wireline acoustic, NMR, and image log data: 39th Ann. Logging Symp., Soc. Prof. Well Log Analysts, paper KK.
Timur, A., 1969, Pulsed nuclear magnetic resonance studies of porosity, movable fluid, and permeability of sandstones: J. Petr. Tech., **21**, 775–786.
Walsh, J. B., and Brace, W. F., 1984, The effect of pressure on porosity and the transport properties of rocks: J. Geophys. Res., **89**, 9425–9431.
Zick, A. A., and Homsy, G. M., 1982, Stokes flow through periodic arrays of spheres: J. Fluid Mech., **115**, 13–26.

APPENDIX

MATHEMATICAL PROCEDURE FOR COMPUTING FORMATION FACTOR

We briefly describe below the mathematical procedure for computing the formation factor of a fluid-saturated porous medium. For a more detailed description, please refer to Bergman and Dunn (1992) and related references.

Consider a sample of periodic porous structure made of solid spheres where the pore space is filled with water. The sample fills up the entire volume in between the plates of an infinite parallel-plate capacitor of thickness L with plates perpendicular to the z-axis. In order to calculate the bulk effective dielectric constant of the composite ϵ_e or the bulk effective conductivity σ_e, we first use an integral equation for the electric potential $\phi(\mathbf{r})$:

$$\phi(\mathbf{r}) = z + \frac{1}{s}\hat{\Gamma}\phi, \qquad (A\text{-}1)$$

where

$$s \equiv \frac{\sigma_w}{\sigma_w - \sigma_m}, \qquad (A\text{-}2)$$

$$\hat{\Gamma}\phi \equiv \int dV'\theta_m(\mathbf{r}')\nabla' G(\mathbf{r}, \mathbf{r}') \cdot \nabla'\phi(\mathbf{r}'), \qquad (A\text{-}3)$$

and where σ_w and σ_m are the conductivities of water and the solid matrix, respectively, $G(\mathbf{r}, \mathbf{r}')$ is a Green's function for the Laplace equation of the electric potential, $\theta_m(\mathbf{r}')$ is the characteristic function which defines the domain of solid matrix, and $\hat{\Gamma}$ is a linear operator which depends on the microgeometry of the porous medium through $\theta_m(\mathbf{r}')$. We have assumed the average electric field is equal to 1. Hence, the first term for the electric potential is simply equal to z, the coordinate. The $\hat{\Gamma}$ operator is made self-adjoint by defining the scalar product of two (scalar) functions as follows:

$$\langle \phi \,|\, \psi \rangle \equiv \frac{1}{V} \int dV \theta_m \nabla \phi^* \cdot \nabla \psi, \qquad (A\text{-}4)$$

where V is the total volume under consideration. The bulk effective conductivity of the composite σ_e is calculated from

$$F(s) \equiv 1 - \frac{\sigma_e}{\sigma_w} = \frac{1}{s} \langle z \,|\, \phi \rangle = \left\langle z \left| \frac{1}{s - \hat{\Gamma}} \right| z \right\rangle. \qquad (A\text{-}5)$$

Because $\hat{\Gamma}$ has a complete set of eigenfunctions ϕ_n with real eigenvalues s_n,

$$\hat{\Gamma}\phi_n = s_n \phi_n, \qquad (A\text{-}6)$$

Equation (A-5) can be transformed into

$$F(s) = \sum \frac{F_n}{s - s_n}, \qquad F_n \equiv |\langle z \,|\, \phi_n \rangle|^2, \qquad (A\text{-}7)$$

where the following inequalities are also satisfied:

$$0 \le s_n < 1, \qquad F(1) \le 1, \qquad \sum F_n \le 1. \quad (A\text{-}8)$$

Expanding $F(s)$ in powers of $1/s$ from equation (A-7), we get

$$F(s) = \frac{\sum F_n}{s} + \frac{\sum s_n F_n}{s^2} + \cdots + \frac{\sum s_n^{r-1} F_n}{s^r} + \cdots. \quad (A\text{-}9)$$

When comparing this to a similar expansion of equation (A-5), we find that

$$\sum s_n^r F_n = \langle z | \hat{\Gamma}^r | z \rangle. \qquad (A\text{-}10)$$

For a periodic porous medium, we can expand the eigenfunctions ϕ_n in Fourier series, and the operator $\hat{\Gamma}$ is then represented by an infinite matrix. The right-hand side of equation (A-10) can then be evaluated by a sequence of matrix-vector products without ever having to evaluate a matrix-matrix product.

This permits us to include a very large number of Fourier components in the calculation, leading to very large matrices $\hat{\Gamma}$. This is necessary in order to ensure good convergence of the calculation and accurate results for the formation factor.

Using these computed moments as input information, we can construct a continued fraction expansion for $F(s)$ and obtain a sequence of successively tighter, converging bounds for $F(s)$. With the formation factor $\mathcal{F}$ defined as

$$\mathcal{F} \equiv \lim_{\sigma_m \to 0} \left(\frac{\sigma_e}{\sigma_w} \right)^{-1} = \frac{1}{1 - F(1)}, \qquad (A\text{-}11)$$

similar converging bounds are calculated for $\mathcal{F}$, and the results are shown in Table A-1.

The calculation involved computation of 20 moments of $F(s)$, which was carried out using reciprocal lattice vectors $\mathbf{g} = (2\pi/d)(n_x, n_y, n_z)$, where d is the lattice constant and n_x, n_y, n_z are integers ranging from $-N$ to $+N$. We used $N = 19$ and 21 (two values of N are always used, and the results are then extrapolated to $N = \infty$ assuming a linear dependence on $1/N$). Upper and lower bounds (bound 2 and bound 1 in Table A-1) were calculated using r lowest moments of $F(s)$. Thus the bounds obtained for $r = 0$ used only the zero moment $\sum F_n$ as input information. As more and more moments are used in the calculation (i.e., as r increases), the bounds get progressively tighter. When r exceeded 11, we usually encountered a situation where small errors in the lower moments caused the continued fraction expansion to terminate (this is discussed in detail in Bergman and Dunn, 1992). Even before that happened, the lower bound (bound 1) already seemed to be well converged with increasing r. A separate calculation carried out using $N = 25$ and 27 did not result in significantly better results. Therefore, in order to reduce computation time, all subsequent calculations involved only 11 moments using $N = 19$ and 21.

Notice that the gap between the upper and lower bounds on the formation factor in Table A-1, obtained using 11 moments, are within 1% of each other when $s = 1.01$, which corresponds to a conductivity ratio $\sigma_m/\sigma_w \approx 0.01$. This means that, at this porosity and this conductivity ratio, the formation factor can be accurately determined to within 1%. However, as s gets closer to 1, the convergence of bound 2 (the upper bound) becomes poorer. Already from this behavior, we may conclude that bound 1 (the lower bound) is closer to the exact result. The poor convergence of the upper bounds on $F(s)$ and $\mathcal{F}$ can

Table A-1. Results for the bounds for the formation factor for a simple cubic array of identical, slightly overlapping spheres with a porosity $\phi = 0.47$.

r	$s = 1.0001$		$s = 1.001$		$s = 1.01$	
	Bound 1	Bound 2	Bound 1	Bound 2	Bound 1	Bound 2
0	2.13	5301.00	2.13	531.00	2.10	54.00
1	2.69	2733.36	2.69	274.59	2.64	28.71
2	2.85	1026.63	2.85	104.55	2.79	12.32
3	2.92	410.23	2.92	43.29	2.85	6.56
4	2.95	173.20	2.94	19.78	2.88	4.39
5	2.97	73.20	2.96	9.89	2.89	3.50
6	2.97	42.49	2.97	6.86	2.90	3.23
7	2.98	17.70	2.97	4.41	2.90	3.02
8	2.98	12.34	2.97	3.89	2.90	2.97
9	2.98	7.89	2.97	3.45	2.90	2.94
10	2.98	6.60	2.97	3.32	2.90	2.93
11	2.98	5.00	2.97	3.17	2.90	2.92

be understood as follows. When s is close to 1, it means that the conductivity ratio σ_m/σ_w is very small. In that case, if the pore space is connected, then the bulk effective conductivity σ_e is finite and of the same order of magnitude as σ_w, even when $\sigma_m = 0$. Consequently, $F(1)$ will be strictly less than 1. However, by a small change in the microstructure, it is possible to disconnect the pore space in neighboring unit cells, in which case we would get $\sigma_e = 0$ and $F(1) = 1$. This could happen even though the changes in the series expansion coefficients of equation (A-9) are very small. That is why the upper bound on $F(1)$ will always be 1, and the upper bound on $F(1.0001)$ converges to the correct value very slowly with increasing r. Because we typically have $\sigma_m/\sigma_w \approx 10^{-6}$, we will always try to approximate $\mathcal{F}$ by using the limiting behavior of its lower bound for $r \to \infty$ and $s \to 1$. Thus, for $\phi = 0.47$, we deduce from Table A-1 that $\mathcal{F} = 2.98$.

When the porosity gets smaller, the convergence becomes progressively poorer and extremely sensitive to the conductivity ratio. Table A-2 shows the result of the formation factor calculation for a simple cubic array of identical overlapping spheres with a porosity of $\phi = 0.06$. As before, we again choose the lower bound as being closer to the correct value for the system. This is also corroborated by the following exercise in which we switch the roles of solid matrix and pore space and calculate the function

$$H(t) \equiv 1 - \frac{\sigma_e}{\sigma_m} = \frac{\mathcal{A}}{t} + \sum_{t_n \neq 0} \frac{H_n}{t - t_n}, \qquad \text{(A-12)}$$

where

$$t = \frac{\sigma_m}{\sigma_m - \sigma_w} \qquad \text{(A-13)}$$

and

$$\mathcal{A} = \frac{1}{\mathcal{F}} = \left.\frac{\sigma_e}{\sigma_w}\right|_{\sigma_m = 0} = \lim_{t \to 0} t H(t). \qquad \text{(A-14)}$$

The residue of the pole at $t = 0$ is just the reciprocal of the formation factor (Korringa, 1984; Korringa and LaTorraca, 1986). This is a property $H(t)$ must have because the pore space is connected. Instead of computing $t H(t)$ for $t = -0.0001$, we calculate the entire pole spectrum for $H(t)$ (not shown here). We used 11 moments and $N = 27$ and 29 for the calculation. The resulting approximant to $H(t)$ has five poles between 0 and 1, in addition to the percolation (or connectivity) related pole at $t = 0$. The formation factor estimated from the pole amplitude at $t = 0$ (i.e., 107) is very close to the lower bound shown in Table A-2.

Table A-2. Results for the formation factor for a simple cubic array of identical overlapping spheres with a porosity $\phi = 0.06$ calculated at finite reciprocal lattice sizes ($N = 19$ and 21).

	$s = 1.0001$		$s = 1.001$		$s = 1.01$	
r	Bound 1	Bound 2	Bound 1	Bound 2	Bound 1	Bound 2
0	16.64	9401.00	16.41	941.00	14.43	95.00
1	24.44	8394.13	23.93	840.55	19.80	85.19
2	48.44	8112.86	46.30	812.58	32.22	82.54
3	57.71	7468.02	54.63	748.78	35.80	76.79
4	77.87	7206.04	72.17	723.02	41.93	74.61
5	87.83	6730.79	80.54	676.65	44.31	70.94
6	94.74	6148.49	86.22	620.56	45.74	66.99
7	100.04	5529.18	90.51	561.88	46.73	63.40
8	101.80	4244.28	91.91	443.54	47.03	57.57
9	109.06	4021.10	97.62	423.45	48.12	56.74
10	111.74	3523.57	99.68	379.30	48.47	55.09